

Superconducting pairing symmetry on the extended Hubbard model in the presence of the Rashba-type spin-orbit coupling

Keisuke Shigeta, Seiichiro Onari, and Yukio Tanaka

Department of Applied Physics, Nagoya University, Nagoya 464-8603, Japan

In order to study the pairing symmetry in non-centrosymmetric superconductors, we solve the linearized Éliashberg's equation on the two-dimensional extended Hubbard model in the presence of the Rashba-type spin-orbit coupling (RSOC) within the random phase approximation. In the presence of the RSOC, three types of pairing symmetries appear in the phase diagram with respect to the on-site Coulomb repulsion U and off-site one V . Each of pairing symmetries is admixture of spin-singlet and -triplet ones. On the basis of analytical study, it is found that the admixture of spin-singlet and -triplet components depends on not only the predominant pairing symmetry but also dispersion relation and pairing interaction.

I. INTRODUCTION

Since the discovery of superconductors without the inversion symmetry in CePt_3Si ,¹ non-centrosymmetric superconductors has been studied intensively as unconventional superconductors. In particular, theoretical studies suggest interesting properties of non-centrosymmetric superconductors such as the magnetoelectric effect,²⁻⁶ anisotropic spin susceptibility,⁶⁻¹¹ and the helical vortex state in magnetic fields.^{12,13} Today, there are various relevant systems in two-dimensional electron gas at heterointerface, *e.g.* between SrTiO_3 and LaAlO_3 ,¹⁴ and non-centrosymmetric crystals, *e.g.* CePt_3Si ,¹ UIr ,¹⁵ CeRhSi_3 ,¹⁶ CeIrSi_3 ,¹⁷ CeCoGe_3 ,^{18,19} and $\text{Li}_2\text{Pd}_x\text{Pt}_{3-x}\text{B}$.²⁰⁻²²

In superconductors with the inversion symmetry, pairing symmetry is classified into even- and odd-parity, *i.e.* spin-singlet and -triplet. In the non-centrosymmetric superconductors, on the other hand, admixture of spin-singlet and -triplet pairings is realized.^{2,7,8,23,24} The admixture is induced by the antisymmetric spin-orbit coupling, which is generated by the lack of the inversion symmetry. For example, it has been proposed that admixture of spin-singlet s -wave and spin-triplet p -wave pairings is realized in a non-centrosymmetric heavy fermion superconductor CePt_3Si from both theoretical^{11,25,26} and experimental^{1,27-32} studies.

In particular, non-centrosymmetric heavy fermion superconductors, *e.g.* CePt_3Si ,¹ UIr ,¹⁵ CeRhSi_3 ,¹⁶ CeIrSi_3 ,¹⁷ and CeCoGe_3 ,^{18,19} are of interest because the superconductivity originates from the Coulomb repulsion. However, there are few theoretical studies on these materials on the basis of the microscopic calculation.^{11,25,33,34} It is desired to microscopically understand the admixture of spin-singlet and -triplet pairings in non-centrosymmetric superconductors where Coulomb repulsion mediates pairing in more detail.

In order to study the above admixture, it is valuable to employ the extended Hubbard model because this model exhibits various pairing symmetries in the presence of the inversion symmetry.³⁵⁻⁴⁷ On the extended Hubbard model, the off-site Coulomb repulsion is considered in addition to the on-site one. It is well known that, while the

on-site Coulomb repulsion induces the spin fluctuation, the charge fluctuation coexists with the spin fluctuation by introducing the off-site Coulomb repulsion.³⁵⁻⁴⁷ Due to the coexistence of the charge fluctuation with the spin one, especially on a two-dimensional square lattice near half-filling, three types of pairing symmetries, *i.e.* spin-singlet $d_{x^2-y^2}$ -wave, spin-triplet f -wave, and spin-singlet d_{xy} -wave ones, compete against each others.³⁵

In the present study, in order to clarify pairing symmetry in non-centrosymmetric superconductors where the Coulomb repulsion mediates pairing, we investigate the two-dimensional extended Hubbard model in the presence of the Rashba-type spin-orbit coupling (RSOC)⁴⁸ on the basis of the random phase approximation (RPA). The RSOC induces breakdown of the inversion symmetry and admixture of pairing symmetry.

The admixture of pairing symmetry has already been studied on the extended Hubbard model in the presence of the RSOC on the basis of the RPA by Yokoyama *et al.*³⁴ However, they investigated only the region where the off-site Coulomb repulsion is small, *i.e.* spin-singlet $d_{x^2-y^2}$ -wave pairing state is stable in the absence of the RSOC. Moreover, there were two simplifications in the pairing interaction. One is that they neglect cross terms of the bubble- and ladder-type diagrams, which are generated by the off-site Coulomb repulsion and the RSOC. The other is that the ladder-type diagrams with the off-site Coulomb repulsion are excluded. In the present study, there is no simplification described above.

The present paper is organized as follows. In §II, we formulate the linearized Éliashberg's equation on the extended Hubbard model in the presence of the RSOC on the basis of the RPA. In §III A, we show results obtained by the numerical calculation within the RPA. After that, we discuss the pairing symmetry on the basis of analytical study in §III B. The summary is given in §IV.

II. FORMULATION

We start with the two-dimensional extended Hubbard model in the presence of the RSOC. The Hamiltonian is

given by

$$\begin{aligned} \mathcal{H} &= \sum_{\mathbf{k},s} \varepsilon_{\mathbf{k}} c_{\mathbf{k}s}^\dagger c_{\mathbf{k}s} + U \sum_i n_{i\uparrow} n_{i\downarrow} + V \sum_{\langle i,j \rangle, s, s'} n_{is} n_{js'} \\ &\quad - \lambda \sum_{\mathbf{k}, s, s'} [\mathbf{g}(\mathbf{k}) \cdot \hat{\boldsymbol{\sigma}}]_{ss'} c_{\mathbf{k}s}^\dagger c_{\mathbf{k}s'}, \quad (1) \\ \varepsilon_{\mathbf{k}} &= -2t(\cos k_x + \cos k_y) - 4t' \cos k_x \cos k_y - \mu, \quad (2) \end{aligned}$$

where $c_{\mathbf{k}s}^{(\dagger)}$ is an annihilation (a creation) operator for an electron with spin s and momentum \mathbf{k} , n_{is} is a number operator for an electron with spin s at site i , and $\langle i, j \rangle$ denotes a set of the nearest neighbor sites. $\varepsilon_{\mathbf{k}}$ is the dispersion relation, where $t^{(l)}$ is the (second) nearest neighbor hopping on a square lattice and μ is the chemical potential. We consider the on-site Coulomb repulsion U and the off-site one V between the nearest neighbor sites. The fourth term is the RSOC, where λ is a magnitude of the RSOC and $\hat{\boldsymbol{\sigma}}$ are the Pauli matrices. The vector $\mathbf{g}(\mathbf{k})$ with the relation $\mathbf{g}(\mathbf{k}) = -\mathbf{g}(-\mathbf{k})$ induces breakdown of the inversion symmetry. We adopt $\mathbf{g}(\mathbf{k}) = (-v_y(\mathbf{k}), v_x(\mathbf{k}), 0)/\bar{v}$ with the quasiparticle velocity $v_{x(y)}(\mathbf{k}) = \partial \varepsilon_{\mathbf{k}} / \partial k_{x(y)} = 2t \sin k_{x(y)} + 4t' \sin k_{x(y)} \cos k_{y(x)}$. $\mathbf{g}(\mathbf{k})$ is normalized by the average velocity \bar{v} which is given by $\bar{v}^2 = \sum_{\mathbf{k}} [v_x(\mathbf{k})^2 + v_y(\mathbf{k})^2] / N$, where N is the number of \mathbf{k} -meshes. The bare Green's function is given by the following 2×2 matrix in spin space,

$$\begin{aligned} \hat{G}(k) &= \begin{pmatrix} G_{\uparrow\uparrow}(k) & G_{\uparrow\downarrow}(k) \\ G_{\downarrow\uparrow}(k) & G_{\downarrow\downarrow}(k) \end{pmatrix} \\ &= \left[(i\omega_n - \varepsilon_{\mathbf{k}}) \hat{\mathbf{I}} + \lambda \mathbf{g}(\mathbf{k}) \cdot \hat{\boldsymbol{\sigma}} \right]^{-1}, \quad (3) \end{aligned}$$

where $\hat{\mathbf{I}}$ is a unit matrix and $k \equiv (i\omega_n, \mathbf{k})$ is an abbreviation. $\omega_n = (2n - 1)\pi T$ is the Matsubara frequency for fermions, where n is an integer and T is temperature.

In order to estimate the pairing instability, we solve the linearized Éliashberg's equation within the RPA

$$\begin{aligned} \alpha \Delta_{s_1 s_2}(k) &= -\frac{T}{N} \sum_{k', c_1, c_2, s_3, s_4} \Gamma_{s_1 s_2 s_3 s_4}^{c_1 c_2}(k - k') \\ &\quad \times P^{c_1}(\mathbf{k}') P^{c_2}(-\mathbf{k}) F_{s_3 s_4}(k'), \quad (4) \end{aligned}$$

$$F_{s_1 s_2}(k) = \sum_{s_3, s_4} G_{s_1 s_3}(k) G_{s_2 s_4}(-k) \Delta_{s_3 s_4}(k), \quad (5)$$

where $\mathbf{P}(\mathbf{k}) = (1, \cos k_x, \sin k_x, \cos k_y, \sin k_y)$ is the phase factor which originates from ladder-type connections with the off-site Coulomb repulsion $V(\mathbf{q}) = 2V(\cos q_x + \cos q_y)$ in the diagrammatic expression. The linearized Éliashberg's equation (4) and (5) is an eigenvalue equation whose eigenvalue and eigenfunction are α and $\hat{\Delta}(k)$, respectively. When the eigenvalue α reaches unity, temperature T corresponds to the superconducting transition temperature T_C . Thus, the eigenvalue α implies the pairing instability with the gap function $\hat{\Delta}(k)$. In solving the linearized Éliashberg's equation, we employ the implicit

restarted Arnoldi method.⁴⁹ This method is powerful in solving an eigenvalue equation with nearly degenerate solutions.

The spin-singlet and -triplet components with $S_z = 0$ are extracted by $[\Delta_{\uparrow\downarrow}(k) \pm \Delta_{\downarrow\uparrow}(k)]/2$, where the sign $+$ ($-$) corresponds to spin-triplet (-singlet) one. The spin-triplet components with $S_z = \pm 1$ are given by $\Delta_{\uparrow\uparrow(\downarrow\downarrow)}(k)$ for the sign $+$ ($-$). In the present paper, we choose the solution whose spin-singlet component is real. The spin-triplet ($S_z = \pm 1$) components are imaginary. The real and imaginary parts of the spin-triplet ($S_z = \pm 1$) components have same amplitude while nodes of the real and imaginary parts have the relation of rotation around $\mathbf{k} = (0, 0)$.

Within the RPA, the effective pairing interaction $\Gamma_{s_1 s_2 s_3 s_4}^{c_1 c_2}(q)$, where $q \equiv (i\nu_m, \mathbf{q})$ with the Matsubara frequency for bosons $\nu_m = 2m\pi T$, is obtained by collecting the infinite series which consist of the irreducible susceptibility in the diagrammatic expression. The irreducible susceptibility is given by

$$\begin{aligned} \chi_{0, s_1 s_2 s_3 s_4}^{c_1 c_2}(q) &= -\frac{T}{N} \sum_{\mathbf{k}} G_{s_1 s_3}(k + q) G_{s_4 s_2}(k) \\ &\quad \times P^{c_1}(\mathbf{k}) P^{c_2}(\mathbf{k}). \quad (6) \end{aligned}$$

The dressed susceptibility is given by

$$\hat{\chi}(q) = \hat{\chi}_0(q) \left[\hat{\mathbf{I}} - \hat{\Gamma}_0(\mathbf{q}) \hat{\chi}_0(q) \right]^{-1}, \quad (7)$$

where the matrices are 20×20 ones with spin indices s_i and phase factor ones c_i defined as

$$\begin{aligned} \hat{M} &= \begin{pmatrix} \hat{M}^{11} & \hat{M}^{12} & \hat{M}^{13} & \hat{M}^{14} & \hat{M}^{15} \\ \hat{M}^{21} & \hat{M}^{22} & \hat{M}^{23} & \hat{M}^{24} & \hat{M}^{25} \\ \hat{M}^{31} & \hat{M}^{32} & \hat{M}^{33} & \hat{M}^{34} & \hat{M}^{35} \\ \hat{M}^{41} & \hat{M}^{42} & \hat{M}^{43} & \hat{M}^{44} & \hat{M}^{45} \\ \hat{M}^{51} & \hat{M}^{52} & \hat{M}^{53} & \hat{M}^{54} & \hat{M}^{55} \end{pmatrix}, \quad (8) \\ \hat{M}^{c_1 c_2} &= \begin{pmatrix} M_{\uparrow\uparrow\uparrow\uparrow}^{c_1 c_2} & M_{\uparrow\uparrow\uparrow\downarrow}^{c_1 c_2} & M_{\uparrow\uparrow\downarrow\uparrow}^{c_1 c_2} & M_{\uparrow\uparrow\downarrow\downarrow}^{c_1 c_2} \\ M_{\uparrow\downarrow\uparrow\uparrow}^{c_1 c_2} & M_{\uparrow\downarrow\uparrow\downarrow}^{c_1 c_2} & M_{\uparrow\downarrow\downarrow\uparrow}^{c_1 c_2} & M_{\uparrow\downarrow\downarrow\downarrow}^{c_1 c_2} \\ M_{\downarrow\uparrow\uparrow\uparrow}^{c_1 c_2} & M_{\downarrow\uparrow\uparrow\downarrow}^{c_1 c_2} & M_{\downarrow\uparrow\downarrow\uparrow}^{c_1 c_2} & M_{\downarrow\uparrow\downarrow\downarrow}^{c_1 c_2} \\ M_{\downarrow\downarrow\uparrow\uparrow}^{c_1 c_2} & M_{\downarrow\downarrow\uparrow\downarrow}^{c_1 c_2} & M_{\downarrow\downarrow\downarrow\uparrow}^{c_1 c_2} & M_{\downarrow\downarrow\downarrow\downarrow}^{c_1 c_2} \end{pmatrix}. \quad (9) \end{aligned}$$

The matrix $\hat{\Gamma}_0(\mathbf{q})$ is given by

$$\hat{\Gamma}_0^{11}(\mathbf{q}) = \begin{pmatrix} -V(\mathbf{q}) & 0 & 0 & -U - V(\mathbf{q}) \\ 0 & U & 0 & 0 \\ 0 & 0 & U & 0 \\ -U - V(\mathbf{q}) & 0 & 0 & -V(\mathbf{q}) \end{pmatrix}, \quad (10)$$

$$\begin{aligned} \hat{\Gamma}_0^{c_1 c_2}(\mathbf{q}) &= \begin{pmatrix} 2V & 0 & 0 & 0 \\ 0 & 2V & 0 & 0 \\ 0 & 0 & 2V & 0 \\ 0 & 0 & 0 & 2V \end{pmatrix} \\ &\quad (c_1 = c_2 = 2 - 5), \quad (11) \end{aligned}$$

$$\hat{\Gamma}_0^{c_1 c_2}(\mathbf{q}) = \hat{0} \quad (c_1 \neq c_2). \quad (12)$$

By using the dressed susceptibility, the effective pairing interaction is expressed as

$$\Gamma_{s_1 s_2 s_3 s_4}^{c_1 c_2}(\mathbf{q}) = - \left[\hat{\Gamma}_0(\mathbf{q}) \hat{\chi}(\mathbf{q}) \hat{\Gamma}_0(\mathbf{q}) \right]_{s_1 s_3 s_4 s_2}^{c_1 c_2} - \Gamma_{0, s_1 s_2 s_3 s_4}^{\prime c_1 c_2}(\mathbf{q}), \quad (13)$$

where the matrix $\hat{\Gamma}'_0(\mathbf{q})$ is given by

$$\hat{\Gamma}_0^{11}(\mathbf{q}) = \begin{pmatrix} -V(\mathbf{q}) & 0 & 0 & 0 \\ 0 & -U - V(\mathbf{q}) & 0 & 0 \\ 0 & 0 & -U - V(\mathbf{q}) & 0 \\ 0 & 0 & 0 & -V(\mathbf{q}) \end{pmatrix}, \quad (14)$$

$$\hat{\Gamma}_0^{\prime c_1 c_2}(\mathbf{q}) = \hat{0} \quad (c_1 \neq 1, c_2 \neq 1). \quad (15)$$

Fig. 1 shows a sense of the formulation for the pairing interaction within the RPA in a diagrammatic representation. In the present RPA for the extended Hubbard

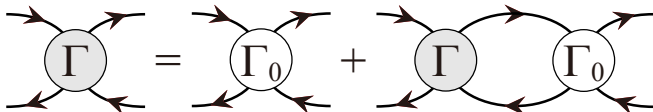


FIG. 1: Diagrammatic sense of the effective pairing interaction $\hat{\Gamma}(\mathbf{q})$ within the RPA. $\hat{\Gamma}_0(\mathbf{q})$ includes the on- and off-site Coulomb repulsions.

model, cross terms of the bubble- and ladder-type diagrams, which generated by the off-site Coulomb repulsion and the RSOC, are taken into account.

Within the RPA, the spin susceptibility is expressed as

$$\chi_{\text{sp}}^{\xi\eta}(\mathbf{q}) = \frac{1}{N} \int_0^\beta d\tau e^{i\nu_m\tau} \langle T_\tau S^\xi(\tau, \mathbf{q}) S^\eta(-\mathbf{q}) \rangle \quad (16)$$

$$= \frac{1}{4} \sum_{s_1, s_2, s_3, s_4} \sigma_{s_3 s_4}^\xi \chi_{s_1 s_2 s_3 s_4}^{11}(\mathbf{q}) \sigma_{s_2 s_1}^\eta, \quad (17)$$

where

$$S^\xi(\mathbf{q}) = \frac{1}{2} \sum_{\mathbf{k}, s, s'} \sigma_{ss'}^\xi c_{\mathbf{k}+\mathbf{q}s}^\dagger c_{\mathbf{k}s'}, \quad (18)$$

$$S^\xi(\tau, \mathbf{q}) = e^{\mathcal{H}\tau} S^\xi(\mathbf{q}) e^{-\mathcal{H}\tau}, \quad (19)$$

with $\xi, \eta = x, y, z$. Similarly, the charge susceptibility is expressed as

$$\chi_{\text{ch}}(\mathbf{q}) = \frac{1}{2N} \int_0^\beta d\tau e^{i\nu_m\tau} \langle T_\tau \rho(\tau, \mathbf{q}) \rho(-\mathbf{q}) \rangle \quad (20)$$

$$= \frac{1}{2} \sum_{s, s'} \chi_{ss's's'}^{11}(\mathbf{q}), \quad (21)$$

where

$$\rho(\mathbf{q}) = \sum_{\mathbf{k}} (c_{\mathbf{k}+\mathbf{q}\uparrow}^\dagger c_{\mathbf{k}\uparrow} + c_{\mathbf{k}+\mathbf{q}\downarrow}^\dagger c_{\mathbf{k}\downarrow}), \quad (22)$$

$$\rho(\tau, \mathbf{q}) = e^{\mathcal{H}\tau} \rho(\mathbf{q}) e^{-\mathcal{H}\tau}. \quad (23)$$

In the present paper, we choose $t = 1$ for a unit of energy. The second nearest neighbor hopping, temperature, and filling are always $t' = 0.1$, $T = 0.04$, and 0.8 electrons per site, respectively, in the actual numerical calculation. We take 64×64 \mathbf{k} -meshes and 1024 Matsubara frequencies.

III. RESULTS

A. Numerical calculation within the RPA

In this subsection, we show results obtained by the numerical calculation within the RPA.

1. In the absence of the RSOC

First, we check the pairing symmetry in the absence of the RSOC, *i.e.* $\lambda = 0$. Fig. 2 shows U - V phase diagram. We identify the pairing symmetry with the largest eigen-

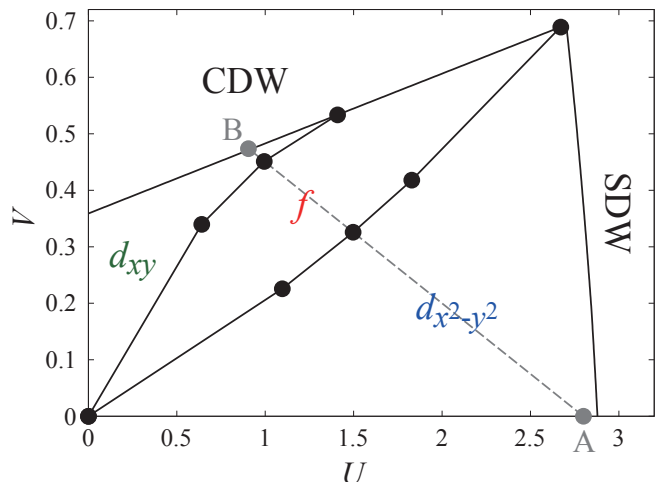


FIG. 2: (Color online) U - V phase diagram in the absence of the RSOC within the RPA. The broken line shows $V = -(U - 2.8)/4$ between points A (2.8, 0) and B (0.9, 0.475).

value α in the linearized Éliashberg's equation (4) and (5) at $T = 0.04$. The boundary with the spin- or charge-density-wave (SDW or CDW) phase is determined by the Stoner's factor, which is defined as the largest eigenvalue of the matrix $\hat{\Gamma}_0(\mathbf{q}) \hat{\chi}_0(\mathbf{q})$ in the dressed susceptibility (7). When the Stoner's factor reaches unity, the dressed susceptibility diverges. In the present paper, we define the SDW or CDW phase as the region where the Stoner's factor reaches 0.98. As shown in Fig. 2, three types of the pairing symmetries can appear by tuning U and V ; spin-singlet $d_{x^2-y^2}$ -wave, spin-triplet f -wave, and spin-singlet d_{xy} -wave pairing symmetries.

Three types of the pairing symmetries are caused by the cooperative/competitive spin and charge susceptibilities controlled by U and V .³⁵ Fig. 3 shows the spin

and charge susceptibilities in the absence of the RSOC on the broken line $V = -(U - 2.8)/4$ in Fig. 2 (U - V space). Here, we plot the maximum values of $\chi_{\text{sp}}^{zz}(q)$ and

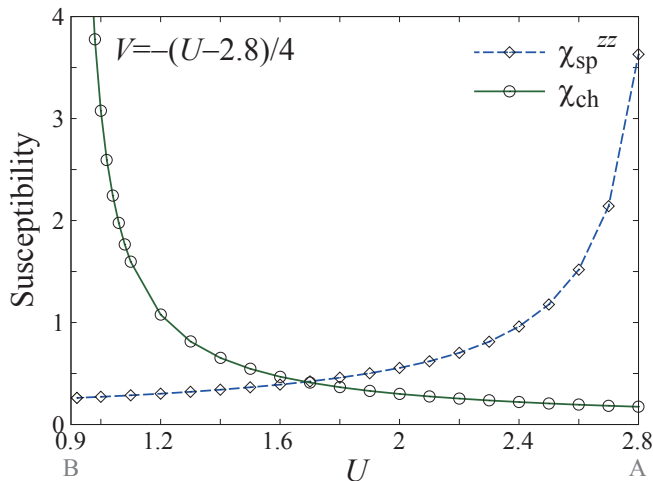


FIG. 3: (Color online) The spin and charge susceptibilities on the broken line $V = -(U - 2.8)/4$ in Fig. 2 (U - V space) without the RSOC. The maximum values are plotted for each (U, V)-point. The result is numerically obtained within the RPA. Points A and B correspond to those in Fig. 2.

$\chi_{\text{ch}}(q)$ for each (U, V)-point. Note that, in the absence of the RSOC, $\chi_{\text{sp}}^{xx}(q) = \chi_{\text{sp}}^{yy}(q) = \chi_{\text{sp}}^{zz}(q)$ and $\chi_{\text{sp}}^{\xi\eta}(q) = 0$ for $\xi \neq \eta$, *i.e.* the spin susceptibility is isotropic. In the region where U (V) is large (small) on the broken line in Fig. 2, the spin susceptibility is dominant as compared to the charge one. In the region where U and V are intermediate on the broken line in Fig. 2, the spin and charge susceptibilities are comparable. In the region where U (V) is small (large) on the broken line in Fig. 2, the charge susceptibility is dominant as compared to the spin one. Thus, surveying from point A to B along the broken line in Fig. 2, dominant fluctuation changes from spin one to charge one.

In the region where U (V) is large (small), dominant spin susceptibility, which is repulsive for spin-singlet pairing channel, generates spin-singlet $d_{x^2-y^2}$ -wave pairing symmetry. This pairing symmetry has the sign change on the Fermi surface through the nesting vector, where the spin susceptibility has peak in momentum space. Thus, for spin-singlet $d_{x^2-y^2}$ -wave pairing symmetry, the spin susceptibility works attractively. In the region where U and V are intermediate, spin-triplet pairing channel exceeds spin-singlet one in the pairing interaction and spin-triplet f -wave pairing symmetry is favored. The reason why spin-triplet pairing channel exceeds spin-singlet one is as follows. In spin-singlet pairing channel, the spin and charge susceptibilities are competitive in the pairing interaction. In spin-triplet pairing channel, on the other hand, the spin and charge susceptibilities are cooperative. In addition, since the pairing interaction for spin-triplet channel is originally attractive, stable pairing symmetry is f -wave one, which has no sign change on the Fermi

surface through the nesting vector, where the spin and charge susceptibilities have peaks in momentum space. In the region where U (V) is small (large), spin-singlet pairing channel and spin-triplet one are comparable in the pairing interaction. Then, the charge susceptibility is attractive for both pairing channels and spin-singlet d_{xy} -wave pairing symmetry is favored. This pairing symmetry has no sign change on the Fermi surface through the nesting vector, where the charge susceptibility has peak in momentum space. The total number of nodes in the gap function for spin-singlet d_{xy} -wave pairing symmetry is less than that for spin-triplet f -wave one. Details have been discussed by Onari *et al.*³⁵

2. In the presence of the RSOC

Next, we introduce the RSOC. It has been known that the RSOC makes the spin susceptibility anisotropic, *i.e.* $\chi_{\text{sp}}^{xx}(q) \neq \chi_{\text{sp}}^{yy}(q) \neq \chi_{\text{sp}}^{zz}(q)$ and $\chi_{\text{sp}}^{\xi\eta}(q) \neq 0$ for $\xi \neq \eta$.⁷ In the presence of the RSOC ($\lambda = 0.3$), the pairing symmetry is shown in Fig. 4. The pairing symmetry and

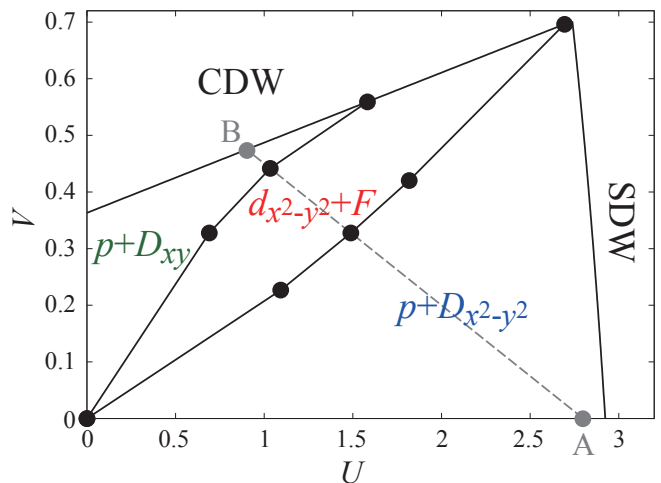


FIG. 4: (Color online) U - V phase diagram in the presence of the RSOC ($\lambda = 0.3$) within the RPA. The broken line shows $V = -(U - 2.8)/4$ between points A (2.8, 0) and B (0.9, 0.475).

boundary with the SDW or CDW phase are determined in the same manner as in the absence of the RSOC. As shown in Fig. 4, three types of pairing symmetries can appear by tuning U and V . In the region where U (V) is large (small), predominantly spin-singlet $d_{x^2-y^2}$ -wave pairing symmetry admixed with spin-triplet ($S_z = \pm 1$) p -wave one is the most stable. We call this pairing symmetry $p + D_{x^2-y^2}$ -wave one in the present paper. Momentum dependence of the gap function is shown in Fig. 5 (a). In the region where U and V are intermediate, predominantly spin-triplet ($S_z = \pm 1$) f -wave pairing symmetry admixed with spin-singlet $d_{x^2-y^2}$ -wave one is the most stable. We call this pairing symmetry $d_{x^2-y^2} + F$ -wave one in the present paper. Momentum dependence

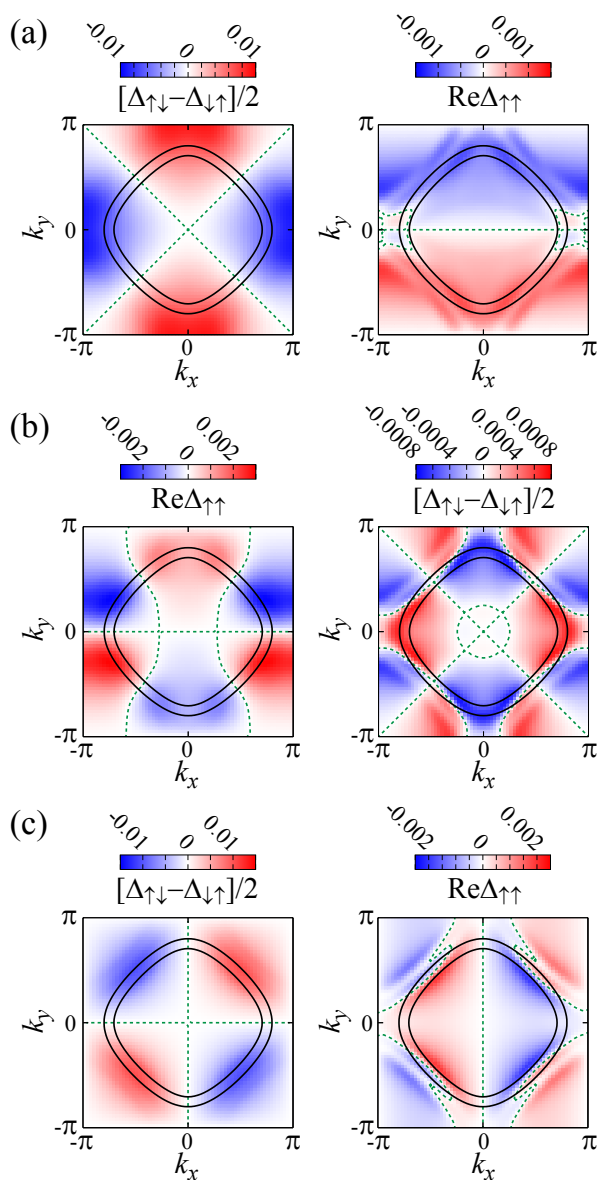


FIG. 5: (Color online) Momentum dependence of the gap functions at $\omega_n = \pi T$ in the presence of the RSOC ($\lambda = 0.3$) within the RPA. (a) $p + D_{x^2-y^2}$ -wave pairing symmetry for $(U, V) = (2.8, 0)$, (b) $d_{x^2-y^2} + F$ -wave one for $(U, V) = (2.1, 0.6)$, and (c) $p + D_{xy}$ -wave one for $(U, V) = (0.8, 0.45)$ are exhibited. Panels on the left (right) side show the predominant components (subcomponents). Black solid lines and green broken ones denote the Fermi surface and node of the gap functions, respectively. For spin-triplet components, only $\text{Re}\Delta_{\uparrow\uparrow}(k)$ is shown.

of the gap function is shown in Fig. 5 (b). In the region where U (V) is small (large), predominantly spin-singlet d_{xy} -wave pairing symmetry admixed with spin-triplet ($S_z = \pm 1$) p -wave one is the most stable. We call this pairing symmetry $p + D_{xy}$ -wave one in the present paper. Momentum dependence of the gap function is shown in Fig. 5 (c). Focusing on the predominant components,

the pairing symmetries are the same as in the absence of the RSOC, *i.e.* spin-singlet $d_{x^2-y^2}$ -wave, spin-triplet f -wave, and spin-singlet d_{xy} -wave pairing symmetries, except lack of spin-triplet component with $S_z = 0$. Phase boundaries are almost unchanged by the RSOC as shown in Figs. 2 and 4. Namely, in the presence of the RSOC, subcomponents are admixed with predominant components whose pairing symmetries are determined by cooperative/competitive spin and charge fluctuations without the RSOC as discussed above. It is discussed later in §III B how the pairing symmetries of the subcomponents are determined.

The eigenvalues α in the linearized Éliashberg's equation (4) and (5) change with U and V in the presence of the RSOC ($\lambda = 0.3$) as shown in Fig. 6, where the data on the broken line $V = -(U - 2.8)/4$ in Fig. 4 (U - V space) are exhibited. In the vicinity of the boundary

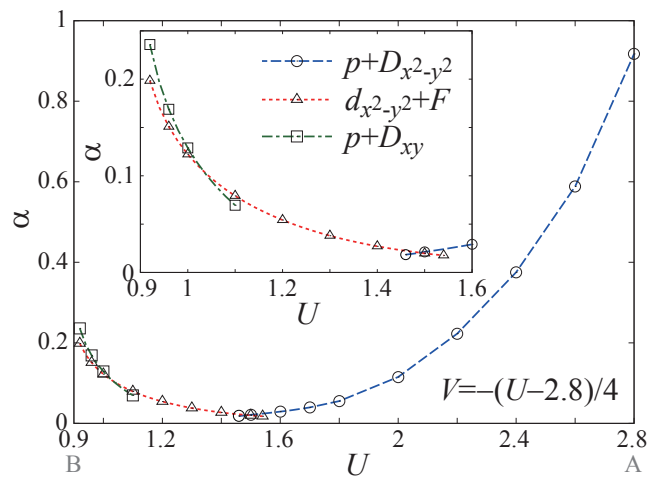


FIG. 6: (Color online) The eigenvalues α in the linearized Éliashberg's equation (4) and (5) on the broken line $V = -(U - 2.8)/4$ in Fig. 4 (U - V space) with $\lambda = 0.3$. The result is numerically obtained within the RPA. Points A and B correspond to those in Fig. 4.

with the SDW or CDW phase, the eigenvalue α is large. Away from the boundary, the eigenvalue α is small. However, even away from the boundary, the eigenvalue α is expected to increase with decreasing temperature.

We also look at ratio between spin-singlet and -triplet ($S_z = \pm 1$) components of the gap function on the broken line $V = -(U - 2.8)/4$ in Fig. 4 (U - V space). Fig. 7 shows the ratio, which is defined by $\kappa \equiv [\Delta_s - \Delta_t] / [\Delta_s + \Delta_t]$. Here, Δ_s and Δ_t denote the maximum absolute values of spin-singlet and -triplet ($S_z = \pm 1$) components, respectively. $\kappa = 1$ corresponds to purely spin-singlet pairing state while $\kappa = -1$ corresponds to purely spin-triplet one. As shown in Fig. 7, the ratio κ slightly depends on U and V in each region, *i.e.* $p + D_{x^2-y^2}$ -wave pairing region ($0.92 \lesssim U \lesssim 1.03$), $d_{x^2-y^2} + F$ -wave pairing one ($1.03 \lesssim U \lesssim 1.48$), and $p + D_{xy}$ -wave pairing one ($1.48 \lesssim U \lesssim 2.8$). Namely,

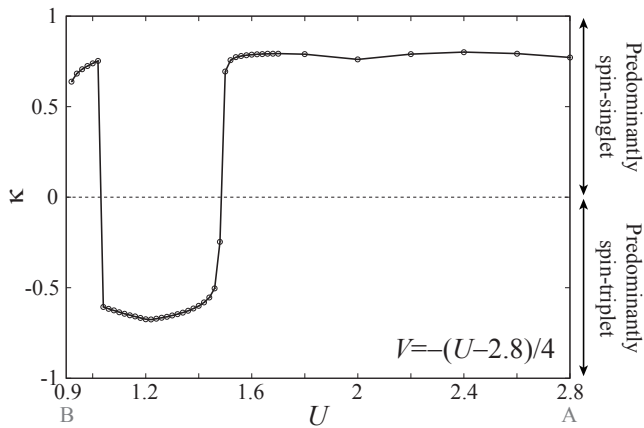


FIG. 7: Ratio κ between spin-singlet and -triplet ($S_z = \pm 1$) components of the gap function on the broken line $V = -(U - 2.8)/4$ in Fig. 4 (U - V space) with $\lambda = 0.3$. The result is numerically obtained within the RPA. Points A and B correspond to those in Fig. 4.

change of pairing interaction slightly affects the ratio κ in each region. The jump of κ on the phase boundaries indicates that phase transitions between different pairing symmetries are not crossover even in the presence of the RSOC.

As functions of λ , the eigenvalue α in the linearized Éliashberg's equation (4) and (5) and the ratio κ between spin-singlet and -triplet ($S_z = \pm 1$) components of the gap function are shown in Figs. 8 and 9, respectively. In both figures, data for $(p+)D_{x^2-y^2}$ -wave

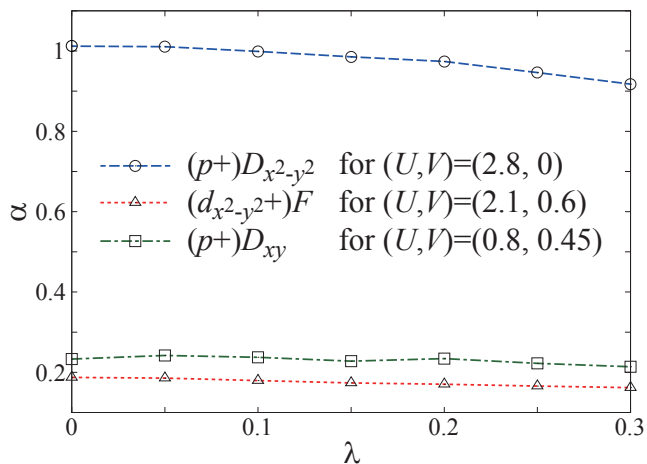


FIG. 8: (Color online) The eigenvalue α in the linearized Éliashberg's equation (4) and (5) as a function of λ for $(p+)D_{x^2-y^2}$ -wave pairing symmetry at $(U, V) = (2.8, 0)$, $(d_{x^2-y^2+})F$ -wave one at $(U, V) = (2.1, 0.6)$, and $(p+)D_{xy}$ -wave one at $(U, V) = (0.8, 0.45)$. The result is numerically obtained within the RPA.

pairing symmetry at $(U, V) = (2.8, 0)$, $(d_{x^2-y^2+})F$ -wave one at $(U, V) = (2.1, 0.6)$, and $(p+)D_{xy}$ -wave one at $(U, V) = (0.8, 0.45)$ are exhibited. As shown in Fig. 8,

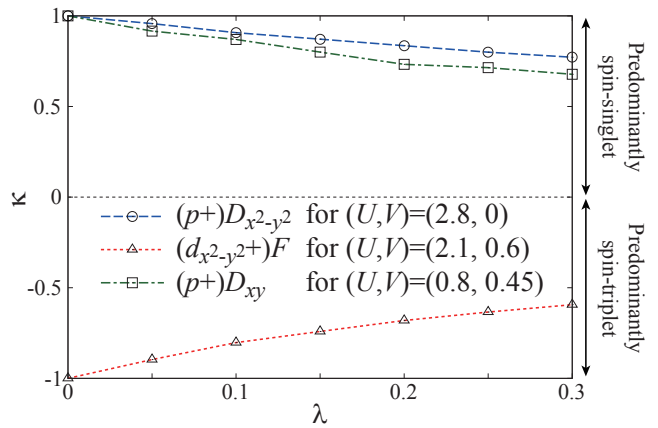


FIG. 9: (Color online) Ratio κ between spin-singlet and -triplet ($S_z = \pm 1$) components of the gap function as a function of λ for $(p+)D_{x^2-y^2}$ -wave pairing symmetry at $(U, V) = (2.8, 0)$, $(d_{x^2-y^2+})F$ -wave one at $(U, V) = (2.1, 0.6)$, and $(p+)D_{xy}$ -wave one at $(U, V) = (0.8, 0.45)$. The result is numerically obtained within the RPA.

the eigenvalue α slightly decreases with increasing λ because the split Fermi surface makes the nesting condition worse. As shown in Fig. 9, the admixture of spin-singlet and -triplet ($S_z = \pm 1$) components is enhanced by λ linearly as discussed later in §III B.

In the above discussion, we mention the pairing symmetry in the presence of the RSOC with focusing on only the predominant component and subcomponent whose amplitude is secondarily large in the gap function. Those always correspond to spin-singlet and -triplet ($S_z = \pm 1$) pairings. However, we also obtain a spin-triplet ($S_z = 0$) component whose amplitude is small as compared to those of the above components. The spin-triplet ($S_z = 0$) component is always an odd function with respect to the Matsubara frequency, so-called odd-frequency pairing state.^{47,50-70} Since Berezinskii proposed the odd-frequency pairing state in 1974,⁵⁰ it has been an important issue in superconductivity/superfluidity. It is expected that the odd-frequency pairing state is discovered in non-centrosymmetric superconductors.

B. Analytical discussion

In this subsection, we discuss the pairing symmetry in the presence of the RSOC analytically. In the previous subsection, it has been clarified that pairing symmetry of the predominant component of the gap function in the presence of the RSOC is the same as in the absence of the RSOC. Now, we focus on pairing symmetry of the admixed subcomponent in the presence of the RSOC. We discuss below how the pairing symmetry of the subcomponent is determined for each predominant pairing symmetry, *i.e.* spin-singlet $d_{x^2-y^2}$ -wave one, spin-triplet ($S_z = \pm 1$) f -wave one, and spin-singlet d_{xy} -wave one.

According to the linearized Éliashberg's equation (5),

if a spin-singlet component is predominant, an admixed spin-triplet ($S_z = 1$) subcomponent of the anomalous Green's function is given by

$$F_{\uparrow\uparrow}^{\text{sub}}(k) = \frac{\lambda \varepsilon_{\mathbf{k}} [-g_x(\mathbf{k}) + i g_y(\mathbf{k})]}{(\omega_n^2 + \varepsilon_{\mathbf{k}}^2)^2} [\Delta_{\uparrow\downarrow}^{\text{dom}}(k) - \Delta_{\downarrow\uparrow}^{\text{dom}}(k)], \quad (24)$$

with expanding the Green's function up to the first order with respect to λ . Here, $F_{ss'}^{\text{sub}}(k)$ and $\Delta_{ss'}^{\text{dom}}(k)$ denote the admixed subcomponent of the anomalous Green's function and the predominant component of the gap function, respectively. Similarly, if a spin-triplet ($S_z = \pm 1$) component is predominant, an admixed spin-singlet subcomponent of the anomalous Green's function is given by

$$\begin{aligned} F_{\uparrow\downarrow}^{\text{sub}}(k) - F_{\downarrow\uparrow}^{\text{sub}}(k) \\ = \frac{4\lambda \varepsilon_{\mathbf{k}}}{(\omega_n^2 + \varepsilon_{\mathbf{k}}^2)^2} [-g_x(\mathbf{k}) \text{Re} \Delta_{\uparrow\uparrow}^{\text{dom}}(k) + g_y(\mathbf{k}) \text{Im} \Delta_{\uparrow\uparrow}^{\text{dom}}(k)]. \end{aligned} \quad (25)$$

Eqs. (24) and (25) indicate that amplitude of an admixed subcomponent increases linearly with λ . This is consistent with the numerical result within the RPA shown in Fig. 9.

From the anomalous Green's function, we can derive the gap function by using the linearized Éliashberg's equation (4). For simplicity, we approximately apply $P^c(\mathbf{k}) = 0$ for $c \neq 1$ hereafter because the pairing symmetry is mainly determined by the term with $P^1(\mathbf{k}')P^1(-\mathbf{k}) = 1$ in the linearized Éliashberg's equation (4) in the actual calculation within the RPA. Then, using the convolution theorem, the linearized Éliashberg's equation (4) is rewritten as

$$\Delta_{ss'}^{\text{sub}}(k) = -\frac{T}{N} \mathcal{F}^{-1} \{ \bar{\Gamma}_{ss'ss'}^{11}(r) \bar{F}_{ss'}^{\text{sub}}(r) \}, \quad (26)$$

$$\bar{\Gamma}_{ss'ss'}^{11}(r) = \mathcal{F} \{ \Gamma_{ss'ss'}^{11}(q) \}, \quad (27)$$

$$\bar{F}_{ss'}^{\text{sub}}(r) = \mathcal{F} \{ F_{ss'}^{\text{sub}}(k) \}, \quad (28)$$

where $\mathcal{F}^{(-1)}$ denotes (inverse) Fourier transformation. In the present subsection, we focus on the pairing symmetry, *i.e.* the nodal structure of the gap function. From this viewpoint, it is available to neglect factors which generate no node in the anomalous Green's function, *i.e.* $\lambda/(\omega_n^2 + \varepsilon_{\mathbf{k}}^2)^2$ in Eq. (24) and $4\lambda/(\omega_n^2 + \varepsilon_{\mathbf{k}}^2)^2$ in Eq. (25). Thus, we can rewrite the anomalous Green's functions as follows,

$$\begin{aligned} \tilde{F}_{\uparrow\uparrow}^{\text{sub}}(k) &= (-2t \cos k_x - 2t \cos k_y - \mu) (\sin k_y + i \sin k_x) \\ &\quad \times [\Delta_{\uparrow\downarrow}^{\text{dom}}(k) - \Delta_{\downarrow\uparrow}^{\text{dom}}(k)], \end{aligned} \quad (29)$$

$$\begin{aligned} \tilde{F}_{\uparrow\downarrow}^{\text{sub}}(k) - \tilde{F}_{\downarrow\uparrow}^{\text{sub}}(k) \\ = (-2t \cos k_x - 2t \cos k_y - \mu) \\ \quad \times [\sin k_y \text{Re} \Delta_{\uparrow\uparrow}^{\text{dom}}(k) + \sin k_x \text{Im} \Delta_{\uparrow\uparrow}^{\text{dom}}(k)], \end{aligned} \quad (30)$$

which are effective in deriving the nodal structure of the gap function, by actually substituting $\varepsilon_{\mathbf{k}}$ and $\mathbf{g}(\mathbf{k})$ in Eqs.

(24) and (25). Here, we neglect t' for simplicity. By using $\tilde{F}_{\uparrow\uparrow}^{\text{sub}}(k)$ and $\tilde{F}_{\uparrow\downarrow}^{\text{sub}}(k) - \tilde{F}_{\downarrow\uparrow}^{\text{sub}}(k)$ instead of $F_{\uparrow\uparrow}^{\text{sub}}(k)$ and $F_{\uparrow\downarrow}^{\text{sub}}(k) - F_{\downarrow\uparrow}^{\text{sub}}(k)$, respectively, in Eq. (28), we can derive the pairing symmetry of the admixed subcomponent of the gap function.

With use of the above analytical discussion, we first discuss $p + D_{x^2-y^2}$ -wave pairing symmetry in the region where U (V) is large (small). In this region, the dominant spin susceptibility mediates predominant spin-singlet $d_{x^2-y^2}$ -wave pairing. We approximate the gap function by $\Delta_{\uparrow\downarrow}^{\text{dom}}(k) - \Delta_{\downarrow\uparrow}^{\text{dom}}(k) = \cos k_x - \cos k_y$. For the given predominant component, we can calculate $\tilde{F}_{\uparrow\uparrow}^{\text{sub}}(k)$ by using Eq. (29). For simplicity, we consider only the real part in $\tilde{F}_{\uparrow\uparrow}^{\text{sub}}(k)$ below. Fig. 10 shows $\bar{F}_{\uparrow\uparrow}^{\text{sub}}(r)$ obtained by Fourier transform (28). Note that this $\bar{F}_{\uparrow\uparrow}^{\text{sub}}(r)$

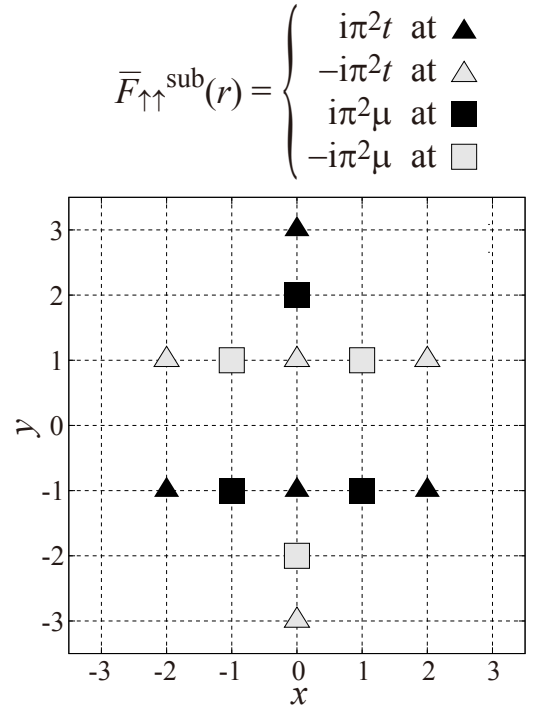


FIG. 10: $\bar{F}_{\uparrow\uparrow}^{\text{sub}}(r)$, which indicates the nodal structure of the admixed spin-triplet ($S_z = 1$) subcomponent of the anomalous Green's function (24), for given predominant spin-singlet $d_{x^2-y^2}$ -wave component approximated by $\Delta_{\uparrow\downarrow}^{\text{dom}}(k) - \Delta_{\downarrow\uparrow}^{\text{dom}}(k) = \cos k_x - \cos k_y$. Note that, strictly speaking, $\bar{F}_{\uparrow\uparrow}^{\text{sub}}(r)$ displayed here corresponds to $\mathcal{F}\{\text{Re} \tilde{F}_{\uparrow\uparrow}^{\text{sub}}(k)\}$.

corresponds to $\mathcal{F}\{\text{Re} \tilde{F}_{\uparrow\uparrow}^{\text{sub}}(k)\}$. There are two kinds of spots in real space. One is the spot whose amplitude increases with $|t|$, which actually depends on materials while it is chosen as a unit of energy in §III A. The other is the spot whose amplitude increases with $|\mu|$. Namely, the pairing symmetry of the admixed subcomponent of the gap function is determined by not only that of the predominant component but also the dispersion relation. On the other hand, the pairing interaction $\bar{\Gamma}_{\uparrow\uparrow\uparrow}^{11}(r)$ for

the admixed spin-triplet ($S_z = 1$) subcomponent has large amplitude at $(x, y) = (0, 0), (\pm 1, 0), (0, \pm 1)$ in this (U, V) region within the RPA. The value at $(x, y) = (0, 0)$ is negative, *i.e.* attractive, while the values at $(x, y) = (\pm 1, 0), (0, \pm 1)$ are positive, *i.e.* repulsive. Then, the resulting product $\bar{\Gamma}_{\uparrow\uparrow\uparrow}^{11}(r)\bar{F}_{\uparrow\uparrow}^{\text{sub}}(r)$ in Eq. (26) has values at $(x, y) = (0, \pm 1)$. Sign of the value at $(x, y) = (0, 1)$ is opposite to that at $(x, y) = (0, -1)$. This amplitude increases with $|t|$ at $(x, y) = (0, \pm 1)$ as shown in Fig. 10. Thus, the admixed spin-triplet ($S_z = 1$) subcomponent becomes p -wave with $\Delta_{\uparrow\uparrow}^{\text{sub}}(k) \propto \sin k_y$. Note that the above $\Delta_{\uparrow\uparrow}^{\text{sub}}(k)$, which is derived from the real part of $\tilde{F}_{\uparrow\uparrow}^{\text{sub}}(k)$, is real. The imaginary part of $\tilde{F}_{\uparrow\uparrow}^{\text{sub}}(k)$ gives the imaginary part of $\Delta_{\uparrow\uparrow}^{\text{sub}}(k)$, which is also p -wave. By the similar procedure, it is derived that $\Delta_{\downarrow\downarrow}^{\text{sub}}(k)$ is also p -wave. Thus, the admixed spin-triplet ($S_z = \pm 1$) subcomponent is found to be p -wave and the amplitude increases with $|t|$.

Next, we discuss $d_{x^2-y^2} + F$ -wave pairing symmetry in the region where U and V are intermediate. In this region, the comparable spin and charge susceptibilities mediate predominant spin-triplet f -wave pairing. We approximate the gap function by $\Delta_{\uparrow\uparrow}^{\text{dom}}(k) = (\cos k_x - \cos k_y) \sin k_y + i(\cos k_x + \cos k_y) \sin k_x$. For the given predominant component, we can calculate $\bar{F}_{\uparrow\downarrow}^{\text{sub}}(k) - \bar{F}_{\downarrow\uparrow}^{\text{sub}}(k)$ by using Eq. (30). Fig. 11 shows $\bar{F}_{\uparrow\downarrow}^{\text{sub}}(r) - \bar{F}_{\downarrow\uparrow}^{\text{sub}}(r)$ obtained by Fourier transform (28). On the other hand, the pairing interaction $\bar{\Gamma}_{\uparrow\downarrow\uparrow}^{11}(r) = \bar{\Gamma}_{\downarrow\uparrow\downarrow}^{11}(r)$ for the admixed spin-singlet subcomponent has large amplitude at $(x, y) = (0, 0), (\pm 1, 0), (0, \pm 1)$ in this (U, V) region within the RPA. All the values are positive, *i.e.* repulsive. Then, the resulting product $\bar{\Gamma}_{\uparrow\downarrow\uparrow}^{11}(r) [\bar{F}_{\uparrow\downarrow}^{\text{sub}}(r) - \bar{F}_{\downarrow\uparrow}^{\text{sub}}(r)]$ in Eq. (26) has values at $(x, y) = (\pm 1, 0)$ and $(x, y) = (0, \pm 1)$. Signs of the values at $(x, y) = (\pm 1, 0)$ are opposite to those at $(x, y) = (0, \pm 1)$. This amplitude increases with $|\mu|$ at $(x, y) = (\pm 1, 0), (0, \pm 1)$ as shown in Fig. 11. Thus, the admixed spin-singlet subcomponent becomes $d_{x^2-y^2}$ -wave with $\Delta_{\uparrow\downarrow}^{\text{sub}}(k) - \Delta_{\downarrow\uparrow}^{\text{sub}}(k) \propto \cos k_x - \cos k_y$. The amplitude is found to increase with $|\mu|$.

Finally, we discuss $p + D_{xy}$ -wave pairing symmetry in the region where U (V) is small (large). In this region, the dominant charge susceptibility mediates predominant spin-singlet d_{xy} -wave pairing. We approximate the gap function by $\Delta_{\uparrow\downarrow}^{\text{dom}}(k) - \Delta_{\downarrow\uparrow}^{\text{dom}}(k) = \sin k_x \sin k_y$. For the given predominant component, we can calculate $\tilde{F}_{\uparrow\uparrow}^{\text{sub}}(k)$ by using Eq. (29). For simplicity, we consider only the real part in $\tilde{F}_{\uparrow\uparrow}^{\text{sub}}(k)$ below. Fig. 12 shows $\bar{F}_{\uparrow\uparrow}^{\text{sub}}(r)$ obtained by Fourier transform (28). Note that this $\bar{F}_{\uparrow\uparrow}^{\text{sub}}(r)$ corresponds to $\mathcal{F}\{\text{Re}\tilde{F}_{\uparrow\uparrow}^{\text{sub}}(k)\}$. On the other hand, the pairing interaction $\bar{\Gamma}_{\uparrow\uparrow\uparrow}^{11}(r)$ for the admixed spin-triplet ($S_z = 1$) subcomponent has large amplitude at $(x, y) = (0, 0), (\pm 1, 0), (0, \pm 1)$ in this (U, V) region within the RPA. The value at $(x, y) = (0, 0)$ is negative, *i.e.* attractive, while the values at $(x, y) = (\pm 1, 0), (0, \pm 1)$ are positive, *i.e.* repulsive. Then, the resulting prod-

$$\bar{F}_{\uparrow\downarrow}^{\text{sub}}(r) - \bar{F}_{\downarrow\uparrow}^{\text{sub}}(r) = \begin{cases} 2\pi^2 t & \text{at } \blacktriangle \\ -2\pi^2 t & \text{at } \triangle \\ 0.5\pi^2 t & \text{at } \blacktriangledown \\ -0.5\pi^2 t & \text{at } \triangledown \\ 1.5\pi^2 \mu & \text{at } \blacksquare \\ -1.5\pi^2 \mu & \text{at } \square \\ 0.5\pi^2 \mu & \text{at } \blacklozenge \\ -0.5\pi^2 \mu & \text{at } \diamond \end{cases}$$

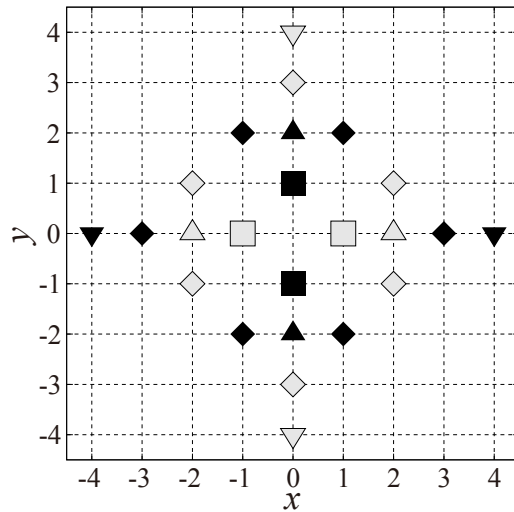


FIG. 11: $\bar{F}_{\uparrow\downarrow}^{\text{sub}}(r) - \bar{F}_{\downarrow\uparrow}^{\text{sub}}(r)$, which indicates the nodal structure of the admixed spin-singlet subcomponent of the anomalous Green's function (25), for given predominant spin-triplet f -wave component approximated by $\Delta_{\uparrow\uparrow}^{\text{dom}}(k) = (\cos k_x - \cos k_y) \sin k_y + i(\cos k_x + \cos k_y) \sin k_x$.

uct $\bar{\Gamma}_{\uparrow\uparrow\uparrow}^{11}(r)\bar{F}_{\uparrow\uparrow}^{\text{sub}}(r)$ in Eq. (26) has values at $(x, y) = (\pm 1, 0)$. Sign of the value at $(x, y) = (1, 0)$ is opposite to that at $(x, y) = (-1, 0)$. This amplitude increases with $|\mu|$ at $(x, y) = (\pm 1, 0)$ as shown in Fig. 12. Thus, the admixed spin-triplet ($S_z = 1$) subcomponent becomes p -wave with $\Delta_{\uparrow\uparrow}^{\text{sub}}(k) \propto \sin k_x$. Note that the above $\Delta_{\uparrow\uparrow}^{\text{sub}}(k)$, which is derived from the real part of $\tilde{F}_{\uparrow\uparrow}^{\text{sub}}(k)$, is real. The imaginary part of $\tilde{F}_{\uparrow\uparrow}^{\text{sub}}(k)$ gives the imaginary part of $\Delta_{\uparrow\uparrow}^{\text{sub}}(k)$, which is also p -wave. By the similar procedure, it is derived that $\Delta_{\downarrow\downarrow}^{\text{sub}}(k)$ is also p -wave. Thus, the admixed spin-triplet ($S_z = \pm 1$) subcomponent is found to be p -wave and the amplitude increases with $|\mu|$.

In the above analytical discussion, we derive the pairing symmetry of the admixed subcomponent of the gap function with use of the simplified pairing interaction, where some dominant modes decomposed in real space are chosen. The derived pairing symmetry is in agreement with that numerically calculated within the RPA in

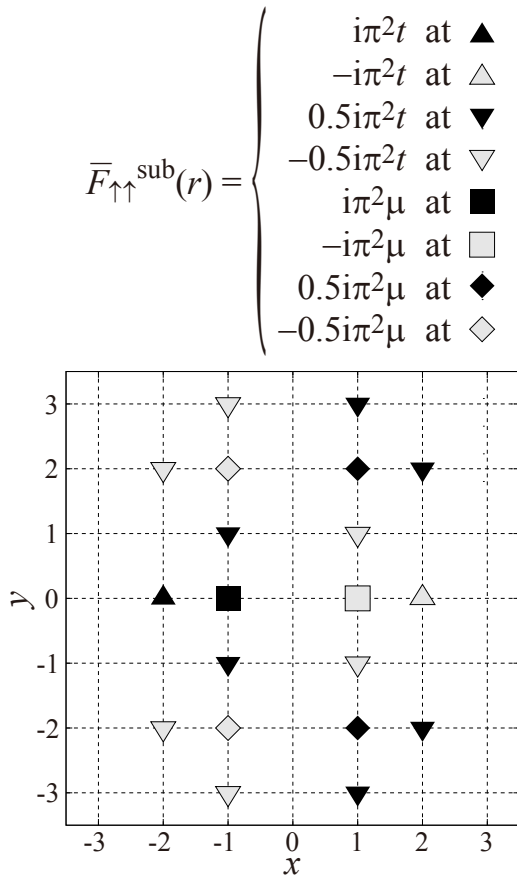


FIG. 12: $\bar{F}_{\uparrow\uparrow}^{\text{sub}}(r)$, which indicates the nodal structure of the admixed spin-triplet ($S_z = 1$) subcomponent of the anomalous Green's function (24), for given predominant spin-singlet d_{xy} -wave component approximated by $\Delta_{\uparrow\downarrow}^{\text{dom}}(k) - \Delta_{\downarrow\uparrow}^{\text{dom}}(k) = \sin k_x \sin k_y$. Note that, strictly speaking, $\bar{F}_{\uparrow\uparrow}^{\text{sub}}(r)$ displayed here corresponds to $\mathcal{F}\{\text{Re}\bar{F}_{\uparrow\uparrow}^{\text{sub}}(k)\}$.

terms of the symmetrical class such as p - or d -wave symmetry. However, there is difference in the nodal structure in detail. The difference comes from the simplification of the pairing interaction. Considering the higher order harmonic components in the pairing interaction, of course, we can reproduce in detail the nodal structure in the admixed subcomponent of the gap function obtained by the numerical calculation within the RPA.

There exists previous analytical discussion on the admixture of the pairing symmetry.⁵ According to the previous study, spin-triplet components are related to spin-singlet one in the gap function by

$$\mathbf{d}(k) \propto \frac{\mathbf{g}(k)}{|\mathbf{g}(k)|} [\Delta_{\uparrow\downarrow}(k) - \Delta_{\downarrow\uparrow}(k)], \quad (31)$$

where $\mathbf{d}(k)$ is the gap function for spin-triplet pairing

state with three components

$$d_x = -\frac{1}{2} [\Delta_{\uparrow\uparrow}(k) - \Delta_{\downarrow\downarrow}(k)], \quad (32)$$

$$d_y = \frac{1}{2i} [\Delta_{\uparrow\uparrow}(k) + \Delta_{\downarrow\downarrow}(k)], \quad (33)$$

$$d_z = \frac{1}{2} [\Delta_{\uparrow\downarrow}(k) + \Delta_{\downarrow\uparrow}(k)], \quad (34)$$

due to degree of freedom of spin. This relation is derived under two assumptions. One is that there is no inter-band pairing between the Fermi surface split by the RSOC. The other is that intra-band pairings on the inner and outer Fermi surface have same pairing symmetry. In the present calculation within the RPA, the former assumption is broken, *i.e.* there is finite inter-band pairing between the Fermi surface split by the RSOC. Therefore, the previous discussion (31) is not applicable. Actually, the previous and present studies give different conclusions. According to the previous study, spin-triplet f -wave pairing symmetry should be admixed with spin-singlet $d_{x^2-y^2}$ -wave one. On the other hand, in the present study on the basis of the RPA, it is derived that spin-triplet ($S_z = \pm 1$) p -wave pairing symmetry is admixed with spin-singlet $d_{x^2-y^2}$ -wave one in the region where U (V) is large (small) as shown in Fig. 4. Thus, in the case where the above two assumptions do not hold, we must take into consideration the dispersion relation and the pairing interaction.

IV. SUMMARY

In order to study the pairing symmetry in non-centrosymmetric superconductors, we have solved the linearized Éliashberg's equation on the two-dimensional extended Hubbard model in the presence of the RSOC within the RPA. We found that three types of the pairing symmetries appeared in the U - V phase diagram in the presence of the RSOC. In the region where U (V) is large (small), $p + D_{x^2-y^2}$ -wave pairing symmetry, which is predominantly spin-singlet $d_{x^2-y^2}$ -wave one admixed with spin-triplet ($S_z = \pm 1$) p -wave one, is the most stable. In the region where U and V are intermediate, $d_{x^2-y^2} + F$ -wave pairing symmetry, which is predominantly spin-triplet ($S_z = \pm 1$) f -wave one admixed with spin-singlet $d_{x^2-y^2}$ -wave one, is the most stable. In the region where U (V) is small (large), $p + D_{xy}$ -wave pairing symmetry, which is predominantly spin-singlet d_{xy} -wave one admixed with spin-triplet ($S_z = \pm 1$) p -wave one, is the most stable.

From analytical study, we found that pairing symmetry of an admixed subcomponent of the gap function depends on not only that of the predominant component but also the dispersion relation and momentum/space dependence of the pairing interaction. Amplitude of the admixed subcomponent of the gap function depends on the dispersion relation, *i.e.* the hopping t and the chemical potential μ , as follows. For the $p + D_{x^2-y^2}$ -wave

pairing symmetry, amplitude of the admixed spin-triplet ($S_z = \pm 1$) p -wave subcomponent increases with $|t|$. For the $d_{x^2-y^2} + F$ -wave pairing symmetry, amplitude of the admixed spin-singlet $d_{x^2-y^2}$ -wave subcomponent increases with $|\mu|$. For the $p + D_{xy}$ -wave pairing symmetry, amplitude of the admixed spin-triplet ($S_z = \pm 1$) p -wave subcomponent increases with $|\mu|$.

V. ACKNOWLEDGMENTS

This work is supported by Grant-in-Aid for Young Scientists (B) No. 22740222 and the "Topological Quantum

Phenomena" (No. 22103005) Grant-in-Aid for Scientific Research on Innovative Areas from the Ministry of Education, Culture, Sports, Science and Technology (MEXT) of Japan. One of the authors (K.S) has been supported by Research Fellowships of the Japan Society for the Promotion of Science for Young Scientists.

-
- ¹ E. Bauer, G. Hilscher, H. Michor, Ch. Paul, E. W. Scheidt, A. Griбанov, Yu. Seropugin, H. Noël, M. Sigrist, and P. Rogl, *Phys. Rev. Lett.* **92**, 027003 (2004).
² V. M. Edelstein, *Sov. Phys. JETP* **68**, 1244 (1989).
³ V. M. Edelstein, *Phys. Rev. Lett.* **75**, 2004 (1995).
⁴ S. K. Yip, *Phys. Rev. B* **65**, 144508 (2002).
⁵ S. Fujimoto, *Phys. Rev. B* **72**, 024515 (2005).
⁶ S. Fujimoto, *J. Phys. Soc. Jpn.* **76**, 034712 (2007).
⁷ L. P. Gor'kov and E. I. Rashba, *Phys. Rev. Lett.* **87**, 037004 (2001).
⁸ P. A. Frigeri, D. F. Agterberg, A. Koga, and M. Sigrist, *Phys. Rev. Lett.* **92**, 097001 (2004).
⁹ P. A. Frigeri, D. F. Agterberg, and M. Sigrist, *New J. Phys.* **6**, 115 (2004).
¹⁰ K. V. Samokhin, *Phys. Rev. Lett.* **94**, 027004 (2005).
¹¹ Y. Yanase and M. Sigrist, *J. Phys. Soc. Jpn.* **77**, 124711 (2008).
¹² R. P. Kaur, D. F. Agterberg, and M. Sigrist, *Phys. Rev. Lett.* **94**, 137002 (2005).
¹³ D. F. Agterberg and R. P. Kaur, *Phys. Rev. B* **75**, 064511 (2007).
¹⁴ N. Reyren, S. Thiel, A. D. Caviglia, L. Fitting Kourkoutis, G. Hammerl, C. Richter, C. W. Schneider, T. Kopp, A.-S. Rüetschi, D. Jaccard, M. Gabay, D. A. Muller, J.-M. Triscone, and J. Mannhart, *Science* **317**, 1196 (2007).
¹⁵ T. Akazawa, H. Hidaka, H. Kotegawa, T. C. Kobayashi, T. Fujiwara, E. Yamamoto, Y. Haga, R. Settai, and Y. Ōnuki, *J. Phys. Soc. Jpn.* **73**, 3129 (2004).
¹⁶ N. Kimura, K. Ito, K. Saitoh, Y. Umeda, H. Aoki, and T. Terashima, *Phys. Rev. Lett.* **95**, 247004 (2005).
¹⁷ I. Sugitani, Y. Okuda, H. Shishido, T. Yamada, A. Thamizhavel, E. Yamamoto, T. D. Matsuda, Y. Haga, T. Takeuchi, R. Settai, and Y. Ōnuki, *J. Phys. Soc. Jpn.* **75**, 043703 (2006).
¹⁸ A. Thamizhavel, H. Shishido, Y. Okuda, H. Harima, T. D. Matsuda, Y. Haga, R. Settai, and Y. Ōnuki, *J. Phys. Soc. Jpn.* **75**, 044711 (2006).
¹⁹ R. Settai, I. Sugitani, Y. Okuda, A. Thamizhavel, M. Nakashima, Y. Ōnuki, and H. Harima, *J. Magn. Magn. Mater.* **310**, 844 (2007).
²⁰ K. Togano, P. Badica, Y. Nakamori, S. Orimo, H. Takeya, and K. Hirata, *Phys. Rev. Lett.* **93**, 247004 (2004).
²¹ P. Badica, T. Kondo, and K. Togano, *J. Phys. Soc. Jpn.* **74**, 1014 (2005).
²² H. Q. Yuan, D. F. Agterberg, N. Hayashi, P. Badica, D. Vandervelde, K. Togano, M. Sigrist, and M. B. Salamon, *Phys. Rev. Lett.* **97**, 017006 (2006).
²³ S. Fujimoto, *J. Phys. Soc. Jpn.* **76**, 051008 (2007).
²⁴ K. Yada, S. Onari, Y. Tanaka, and J. Inoue, *Phys. Rev. B* **80**, 140509(R) (2009).
²⁵ Y. Yanase and M. Sigrist, *J. Phys. Soc. Jpn.* **76**, 043712 (2007).
²⁶ Y. Yanase and M. Sigrist, *J. Phys. Soc. Jpn.* **76**, 124709 (2007).
²⁷ M. Yogi, Y. Kitaoka, S. Hashimoto, T. Yasuda, R. Settai, T. D. Matsuda, Y. Haga, Y. Ōnuki, P. Rogl, and E. Bauer, *Phys. Rev. Lett.* **93**, 027003 (2004).
²⁸ E. Bauer, H. Kaldarar, A. Prokofiev, E. Royanian, A. Amato, J. Sereni, W. Brämer-Escamilla, and I. Bonalde, *J. Phys. Soc. Jpn.* **76**, 051009 (2007).
²⁹ R. Settai, T. Takeuchi, and Y. Ōnuki, *J. Phys. Soc. Jpn.* **76**, 051003 (2007).
³⁰ T. Yasuda, H. Shishido, T. Ueda, S. Hashimoto, R. Settai, T. Takeuchi, T. D. Matsuda, Y. Haga, and Y. Ōnuki, *J. Phys. Soc. Jpn.* **73**, 1657 (2004).
³¹ M. Yogi, H. Mukuda, Y. Kitaoka, S. Hashimoto, T. Yasuda, R. Settai, T. D. Matsuda, Y. Haga, Y. Ōnuki, P. Rogl, and E. Bauer, *J. Phys. Soc. Jpn.* **75**, 013709 (2006).
³² W. Higemoto, Y. Haga, T. D. Matsuda, Y. Ōnuki, K. Ohishi, T. U. Ito, A. Koda, S. R. Saha, and R. Kadono, *J. Phys. Soc. Jpn.* **75**, 124713 (2006).
³³ Y. Tada, N. Kawakami, and S. Fujimoto, *J. Phys. Soc. Jpn.* **77**, 054707 (2008).
³⁴ T. Yokoyama, S. Onari, and Y. Tanaka, *Phys. Rev. B* **75**, 172511 (2007).
³⁵ S. Onari, R. Arita, K. Kuroki, and H. Aoki, *Phys. Rev. B* **70**, 094523 (2004).
³⁶ Y. Tanaka, Y. Yanase, and M. Ogata, *J. Phys. Soc. Jpn.* **73**, 319 (2004).
³⁷ Y. Tanaka, Y. Yanase, and M. Ogata, *J. Phys. Soc. Jpn.* **73**, 2053 (2004).
³⁸ Y. Tanaka and K. Kuroki, *Phys. Rev. B* **70**, 060502(R) (2004).
³⁹ S. Onari, R. Arita, K. Kuroki, and H. Aoki, *J. Phys. Soc. Jpn.* **74**, 2579 (2005).
⁴⁰ K. Kuroki, Y. Tanaka, and R. Arita, *Phys. Rev. B* **71**, 024506 (2005).
⁴¹ K. Kuroki and Y. Tanaka, *J. Phys. Soc. Jpn.* **74**, 1694 (2005).
⁴² K. Kuroki, S. Onari, Y. Tanaka, R. Arita, and T. Nojima,

- Phys. Rev. B **73**, 184503 (2006).
- ⁴³ K. Kuroki, J. Phys. Soc. Jpn. **75**, 051013 (2006).
- ⁴⁴ K. Kuroki, J. Phys. Soc. Jpn. **75**, 114716 (2006).
- ⁴⁵ K. Yoshimi, M. Nakamura, and H. Mori, J. Phys. Soc. Jpn. **76**, 024706 (2007).
- ⁴⁶ T. Aonuma, Y. Fuseya, and M. Ogata, J. Phys. Soc. Jpn. **78**, 034722 (2009).
- ⁴⁷ K. Shigeta, Y. Tanaka, K. Kuroki, S. Onari, and H. Aizawa, Phys. Rev. B **83**, 140509(R) (2011).
- ⁴⁸ E. I. Rashba, Sov. Phys. Solid State **2**, 1109 (1960).
- ⁴⁹ W. E. Arnoldi, Q. Appl. Math. **9**, 17 (1951).
- ⁵⁰ V. L. Berezinskii, JETP Lett. **20**, 287 (1974).
- ⁵¹ K. Yada, S. Onari, and Y. Tanaka, Physica C **469**, 991 (2009).
- ⁵² A. Balatsky and E. Abrahams, Phys. Rev. B **45**, 13125 (1992).
- ⁵³ N. Bulut, D. J. Scalapino, and S. R. White, Phys. Rev. B **47**, 14599 (1993).
- ⁵⁴ P. Coleman, E. Miranda, and A. Tsvetik, Phys. Rev. B **49**, 8955 (1994).
- ⁵⁵ M. Vojta and E. Dagotto, Phys. Rev. B **59**, R713 (1999).
- ⁵⁶ Y. Fuseya, H. Kohno, and K. Miyake, J. Phys. Soc. Jpn. **72**, 2914 (2003).
- ⁵⁷ T. Hotta, J. Phys. Soc. Jpn. **78**, 123710 (2009).
- ⁵⁸ D. Solenov, I. Martin, and D. Mozyrsky, Phys. Rev. B **79**, 132502 (2009).
- ⁵⁹ K. Shigeta, S. Onari, K. Yada, and Y. Tanaka, Phys. Rev. B **79**, 174507 (2009).
- ⁶⁰ H. Kusunose, Y. Fuseya, and K. Miyake, J. Phys. Soc. Jpn. **80**, 044711 (2011).
- ⁶¹ H. Kusunose, Y. Fuseya, and K. Miyake, J. Phys. Soc. Jpn. **80**, 054702 (2011).
- ⁶² Y. Fuseya and K. Miyake, J. Phys. Soc. Jpn. **80**, 054705 (2011).
- ⁶³ K. Shigeta, S. Onari, and Y. Tanaka, Phys. Rev. B **85**, 224509 (2012).
- ⁶⁴ M. Matsumoto, M. Koga, and H. Kusunose, J. Phys. Soc. Jpn. **81**, 033702 (2012).
- ⁶⁵ H. Kusunose, M. Matsumoto, and M. Koga, Phys. Rev. B **85**, 174528 (2012).
- ⁶⁶ F. S. Bergeret, A. F. Volkov, and K. B. Efetov, Phys. Rev. Lett. **86**, 4096 (2001).
- ⁶⁷ Y. Tanaka and A. A. Golubov, Phys. Rev. Lett. **98**, 037003 (2007).
- ⁶⁸ Y. Tanaka, A. A. Golubov, S. Kashiwaya, and M. Ueda, Phys. Rev. Lett. **99**, 037005 (2007).
- ⁶⁹ Y. Tanaka, Y. Tanuma, and A. A. Golubov, Phys. Rev. B **76**, 054522 (2007).
- ⁷⁰ Y. Tanaka, M. Sato, and N. Nagaosa, J. Phys. Soc. Jpn. **81**, 011013 (2012).